

RFA-Cut: Semi-automatic Segmentation of Radiofrequency Ablation Zones with and without Needles via Optimal s-t-Cuts

Jan Egger^{1,2,3}, Harald Busse⁴, Philipp Brandmaier⁴, Daniel Seider⁴, Matthias Gawlitza⁴
Steffen Strocka⁴, Philip Voglreiter¹, Mark Dokter¹, Michael Hofmann¹, Bernhard Kainz⁵
Xiaojun Chen⁶, Alexander Hann⁷, Pedro Boechat¹, Bernd Freisleben², Tuomas Alhonnoro³
Mika Pollari³, Michael Moche⁴, Dieter Schmalstieg¹

¹Institute for Computer Graphics and Vision, Graz University of Technology, Austria

²Distributed Systems Group, Philipp University of Marburg, Germany

³School of Science, Aalto University, Espoo, Finland

⁴Dept. of Diagnostic and Interventional Radiology, Leipzig University Hospital, Germany

⁵Dept. of Computing, Imperial College London, UK

⁶School of Mechanical Engineering, Shanghai Jiao Tong University, Shanghai, China

⁷Dept. of Internal Medicine and Gastroenterology, Katharinenhospital, Stuttgart, Germany

Abstract— In this contribution we present a semi-automatic segmentation algorithm for radiofrequency ablation (RFA) zones via optimal s-t-cuts. Thereby, the interactive graph-based approach builds upon a polyhedron to construct the graph and was specifically designed for computed tomography (CT) acquisitions from patients that had RFA treatments of Hepatocellular Carcinomas (HCC). For evaluation, we used twelve post-interventional CT datasets from the clinical routine and as evaluation metric we utilized the Dice Similarity Coefficient (DSC) - which is commonly accepted for judging computer aided medical segmentation tasks. However, compared with pure manual slice-by-slice expert segmentations from interventional radiologists, we were able to achieve a DSC of about eighty percent, which is sufficient for our clinical needs. Moreover, our approach was able to handle images containing (75.9%) and not containing (78.1%) the RFA needles still in place. Additionally, we found no statistically significant difference ($p < 0.05$) between the segmentation results of the subgroups for a Mann-Whitney test. Finally, to the best of our knowledge, this is the first time that a segmentation approach for CT scans still including the RFA needles is reported and we show why another state-of-the-art segmentation method fails for these cases. However, intraoperative scans including an RFA probe are very critical in the clinical practice and need a very careful segmentation and inspection for under-treatment and therefore possibly resulting in tumor recurrence (up to 40%). However, an additional ablation can still be performed within the same intervention inside the OR with the needle already in place. This avoids patient stress and associated risks of a following intervention at a later date. Ultimately, the segmented ablation zone containing the placed RFA needle, can be used for a precise ablation simulation, as the real needle position is now known.

I. INTRODUCTION

Liver cancer is on the rise worldwide, mainly because of hepatitis infection and alcohol abuse. Especially patients with primary liver cancer (Hepatocellular Carcinomas, HCC) have

a poor prognosis because of its late symptomatic onset resulting in a median survival time of 4 to 6 months from the time of diagnosis when untreated. According to the recent treatment guidelines [1], Radiofrequency ablation (RFA) serves as a first line therapy approach for early HCC in patients with liver cirrhosis. Also for metastatic liver disease, the local usage of ablation therapies increases. While the technique was originally developed for patients who were not eligible for surgery, its use has now expanded to patients as a bridge to liver transplantation and even as an alternative to surgical resection in the early stages of the disease. RFA was first described in the early 1990s, followed by huge technical advances throughout the last decades. The underlying principle is based on a high frequency alternating current which is delivered through one or more electrodes in the treated lesion (Fig. 1.).

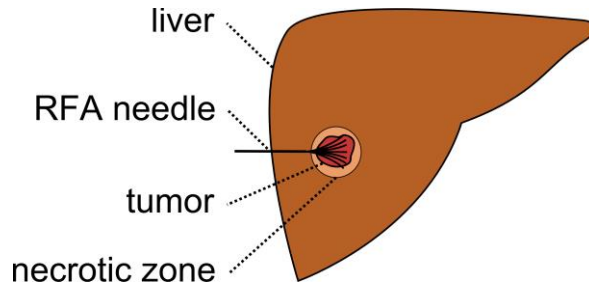


Fig. 1. Schematic view of the liver (brown) with a fully expanded and umbrella-shaped radiofrequency ablation (RFA) needle (back). The needle tips are located in a liver tumor (red) surrounded by the so called necrotic zone (light brown).

Optimally, the heat generated destroys cancer cells by inducing a coagulative necrosis with cellular proteins being denaturated. Most commonly, tissue necrosis already begins at approximately 60°C, but usually, temperatures over 100° are

needed to achieve satisfying results. The amount of destroyed tissue mostly depends on the individual impedance and placement of the needle. Further, it is inversely proportional to the square of the distance from the electrode. As a result, tissue cools rapidly away from the tip of the needle probe. Hence, the proximity to large blood vessels also plays a major role in the heat transmission. Blood flow protects the vessel wall from damage, but on the flipside acts as a heat sink by cooling down nearby tissue limiting the methods overall success. As a consequence of this, a significant mismatch between expected and truly induced lesion size and geometry has been observed in many radiofrequency ablations performed in the liver. It can lead to over-treatment with severe injuries (up to 9% major complications [2]), or under-treatment with tumor recurrence (up to 40% [2]). Tumor recurrence has a major limitation on the survival rates for all types of cancer therapies, i.e., resection and RFA. Cohort patient studies have shown the evidence of a significant reduction in the recurrence rate if the RFA generates a safety rim around the tumor. This elicits the need for a reliable method for the comparison of localization, size and geometry of the tumor in the preoperative images on the one hand, and thermally induced lesion after ablation on the other hand. Tumor recurrence can be diagnosed by the detection of typical alteration in tissue enhancement. Nevertheless, increase of size or geometry of the lesion seems to be a much more sensitive indicator of early recurrence in follow up imaging. Therefore, a reliable and feasible determination of the ablation zone at baseline and follow-up may contribute to a positive outcome for the patient and can lead to a better understanding about the cause of new tumor growth. Consecutively, the additional knowledge might lead to improvement of ablation protocols or even new treatment strategies.

Determination of therapeutically induced lesions after minimally invasive cancer treatment can be performed by segmentation. This is usually done by a time consuming manual procedure and therefore not yet part of the clinical routine. A validated segmentation algorithm may potentially increase the acceptance of the method in the medical community and consecutively lead to a significant benefit in patient treatment.

The segmentation field in computer vision deals with the computer-aided analysis and classification of (medical) image data in a broad range of applications, such as the automatic detection of humans in videos or the automatic volumetry on brain images of patients. In general, the target of a segmentation algorithm is to support and speedup a time-consuming manual selection and contouring process. However, others working in the specific area of (semi-)automatic segmentation of ablation zones in RFA datasets of the liver are Passera et al. [3]. They claim to present the first attempt to obtain a quantitative tool aimed to assess the accuracy of RFA. For the segmentation, they use a Live-Wire algorithm – implemented within the MeVisLab platform (www.mevislab.de) – and clustering. However, they did not include RFA data in their study if the needle was still present

within the scan. But this is the case when the interventionalist particularly wants to assess the size of the induced lesion under the assumption of continuation or an additional ablation. And to avoid the repositioning or the replacement of the instrument, the RFA probe remains in the patient while performing the control scan. Additionally, the segmentation approach worked only in 2D, which can be very time-consuming in case of tumors or ablation zones that extend over many slices; the reported segmentation time was ten minutes. A separate radio frequency ablation registration, segmentation, and fusion tool called RFAST has been presented by McCreedy et al. [4], who also apply a livewire-based method in single 2D slices. However, the segmentation process has not been described in detail and no quantitative segmentation results are presented. Keil et al. [5] have presented their results of the semi-automated segmentation of liver metastases treated by radiofrequency ablation. The segmentation algorithm used in their study consists of six steps where a three-dimensional region growing and morphologic operations, like erosion, dilation are performed. Besides, the user needs to draw a diameter across the lesion, or, for smaller lesions, provide a single click inside the lesion as initialization. Weihsen et al. [6] have introduced a workflow oriented software support for image guided RFA of focal liver malignancies, in which they also segment coagulation necrosis in the (post-interventional) control scans after the ablation. Thereto, the user has to provide a seed point inside the ablation zone which starts a morphology-based region growing algorithm proposed by Kuhnigk et al. [7]. Afterwards, the segmentation result can be corrected towards more “irregular” or “roundish” geometry by manual interaction. Bricault et al. [8] have presented their preliminary results of a 3D shape-based analysis of CT Scans for the detection of local recurrence of liver metastases after RFA treatment. For that purpose, they applied a semi-automated 3D segmentation process that uses a “tagged” watershed algorithm. The semi-automated segmentation, on average, takes about 4 minutes and the minimum required user interaction includes two mouse clicks: one in the ablated tumor and one in the surrounding liver parenchyma. Another volumetric evaluation study of the variability of the size and the shape of necrosis induced by RFA in human livers has been presented by Stippel et al. [9]. The volumetric evaluation was performed with the software package VA 40C from Siemens on a Leonardo workstation. For the stepwise segmentation of the ablation-induced lesions, a region of interest had to be defined in each slice by manually tracking the approximate borders of the lesion. Afterwards, the precise border of the lesion was determined by a filter algorithm (provided by the software package), which is based on density differences between the ablated tissue and the liver tissue. As an enclosure to this section, we want to point the interested reader to an overview publication about computer-assisted planning, intervention and assessment of liver tumor ablation from Schumann et al. [10]. To the best of our knowledge, there is no work that has studied the semi-automatic 3D segmentation of post-interventional RF ablation zones with clinical data that has still the ablation needles in place.

II. MATERIAL AND METHODS

A. Data Acquisition

For this retrospective study we used twelve datasets from ten patients, who underwent a radiofrequency ablation in the liver. All datasets had a matrix size of 512x512 in x- and y-direction, and the number of slices in z direction ranged from 52 to 232. The slice thickness was either 1 or 2 mm, and the pixel spacing ranged from 0.679 to 0.777 with spacing between the slices of 1 to 3 mm. In six datasets, the ablation needle was still present and all datasets have been acquired on multislice CT scanner (Philips Brilliance or Mx8000, Philips Healthcare, Netherlands). The data collection, analysis and a future publication, was approved by the Institutional Review Board (IRB) of the Leipzig University Hospital (reference number: 381-14-15122014) and will be provided to the research community shortly on our ClinicImpact project page:

<http://www.clinicimpact.eu/>

However, medical ablation datasets from a comprehensive pig study can already be found on the webpage of our European Project *GoSmart* [11]:

<http://www.gosmart-project.eu/>

B. Manual Segmentation

To generate the Ground Truth of the ablation zones, we set up a segmentation framework under MeVisLab which provided simple contouring capabilities. This allowed the physicians to manually outline RFA lesions in the datasets slice-by-slice without any algorithmic support to avoid distortions. Afterwards, the single contours were voxelized and then merged to a 3D mask representing the ablation zone. These 3D masks have been used for comparison and quantitative evaluation with the semi-automatic segmentation results.

C. Evaluation Metric

As an evaluation metric we used the Dice Similarity Coefficient (DSC). The DSC is a common metric widely used in medical image analysis where the agreement between two binary volumes M and S is calculated:

$$DSC = \frac{2 \cdot V(M \cap S)}{V(M) + V(S)} \quad (1)$$

Here, M and S are the binary masks from the manual (M) and the semi-automatic (S) segmentations, $V(\cdot)$ denotes the volume (in cm^3) and (\cap) denotes the intersection. We computed the volume by counting the number of voxels and multiplying them with the physical size of voxels. In addition to the DSC, we measured the time it took an experienced radiologist to manually outline the ablation zones and

compared it with the computation time of our semi-automatic segmentation.

D. Semi-automatic Segmentations

The semi-automatic segmentation algorithm uses a spherical template to set up a three-dimensional graph $G(V,E)$ around the ablation zone [12]. Overall, the Graph consists of nodes $n \in V$ and edges $e \in E$ connecting these nodes, and a source s and a sink t . Thereby, the nodes are sampled along rays whose origin resides at a user-defined seed point while their direction points towards the surface of a polyhedron enclosing the seed point. After graph construction, the segmentation result is calculated by dividing the graph into two sets of nodes via a Min-Cut/Max-Flow algorithm [13]. As a result, one set of nodes represents the ablation zone (foreground) and the other set represents the surrounding structures (background). Amongst others, the basic segmentation scheme has already been successfully applied to pituitary adenomas [14] and the prostate central glands [15]. Following, the segmentation scheme was later turned into an interactive real-time approach [16] and for this study it was enhanced by an additional refinement option [17]. For starting the interactive segmentation process, the user places a seed point roughly in the middle of the ablation zone on a 2D slice. From this seed point we construct the graph and automatically calculate and display the segmentation result for the user. The user now has the option to drag the seed point around to interactively generate new segmentation results depending on the current seed point positions. Additionally, the user can interrupt the dragging of the seed point by releasing the mouse button and add an arbitrary amount of seed points on the border of the ablation zone. Thus, the algorithm gets supporting input about the location of the border and steers the behavior of the min-cut. However, the user can always come back to the initial seed point and start dragging it around the image again (note: additional placed seed points will not get lost then. Rather these stay fixed and continue to influence/restrict the min-cut). The overall workflow of the segmentation scheme is presented in Fig. 2.

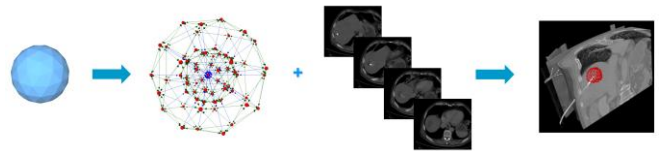


Fig. 2. Overall workflow of the RF ablation zone segmentation: a sphere (left) is used to construct a graph (second image from the left). The graph is constructed (not visible to the user) at the user-defined seed point position within the image (third image from the left). Finally, the segmentation result (red) corresponding to the see point is shown to the user (rightmost image).

III. RESULTS

The proposed interactive segmentation algorithm has been implemented as a C++ module (Visual Studio 2008) for the medical prototyping platform MeVisLab. The computation of

the segmentation result, including the graph construction from the current user-defined seed point position and the optimal min-cut calculation could be performed within one second (on a laptop with Intel Core i5-750 CPU, 4 × 2.66 GHz, 8 GB RAM, Windows 7 Professional x64 Version with Service Pack 1 installed). This enables real-time feedback of our algorithm presented to the user. This immediate response and feedback of the segmentation allows user guidance of the algorithm to a satisfying outcome.

Fig. 3. presents a semi-automatic segmentation result of a post-interventional ablation zone for visual inspection. As the CT data has been acquired immediately after the treatment, the needle used for the ablation is still in place and therefore visible in the scan. The left image shows the axial slice with a user-defined seed point (blue) and the red dots are the border of the segmentation in this slice. The red dots represent the last nodes of the graph that are still bound to the source s after the min-cut. The image in the middle presents the segmentation result in 3D. Again, the red dots show the last nodes of the graph which are still connected to the source after applying the min-cut. Finally, the rightmost image visualizes a closed surface (green) that has been generated from the graph's nodes representing the segmentation result. Afterwards, this closed surface is used to generate a solid mask for the calculation of the DSC with the pure manual slice-by-slice segmentations.

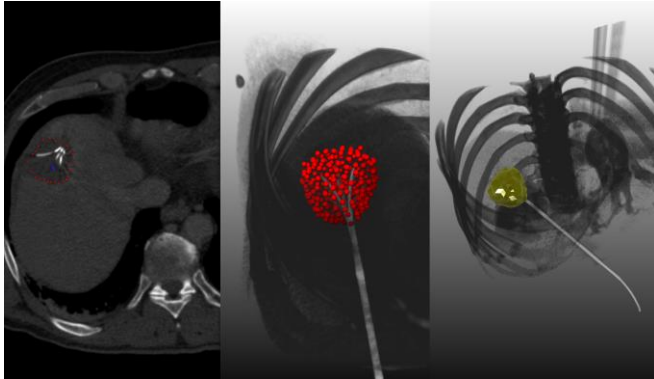


Fig. 3. Semi-automatic segmentation result of an RFA zone in a post-interventional CT scan, where the ablation needle is still in place, for visual inspection. The left image shows the axial slice where the user-defined seed point (blue) has been placed, additionally, the corresponding segmentation result (red dots) is shown. Thereby, the red dots are the last nodes of the graph that are still bound to the source s after the mincut. The image in the middle shows a 3D view of all nodes (red dots) that describe the surface of the segmented ablation zone after the mincut. Furthermore, the rightmost image displays a closed surface (green) of the segmentation result (the red dots from the previous image). The closed surface of the segmentation result is used to generate a solid mask for calculation of the DSC with the pure manual slice-by-slice expert segmentations.

Tab. 1. and Tab. 2. present the direct comparison of manual slice-by-slice segmentations from physician 1 and 2 with results of the semi-automatic segmentations for twelve ablation zones using the DSC. Furthermore, Tab. 3. presents the direct comparison of manual slice-by-slice segmentations

from physician 1 and physician 2 for the twelve ablation zones also via the Dice Similarity Coefficient.

	Volume (cm ³)		Number of Voxel		DSC (%)
	manual 1	semi	manual 1	semi	
Range	10.0	6.3	5866	3689	71.8
	122.6	104.0	70806	70208	83.5
μ	35.9	33.0			77.0
\pm	\pm	\pm	31294.8	30756.3	\pm
σ	30.0	25.1			4.7

Tab. 1. Direct comparison of manual slice-by-slice segmentations from physician 1 and semi-automatic segmentation results for twelve ablation zones via the DSC.

	Volume (cm ³)		Number of Voxel		DSC (%)
	manual 2	semi	manual 2	semi	
Range	11.1	6.3	6543	3689	68.1
	117.7	104.0	67963	70208	85.3
μ	36.2	33.0			77.1
\pm	\pm	\pm	31240.1	30756.3	\pm
σ	28.7	25.1			5.8

Tab. 2. Similar to Tab. 1. the direct comparison with physician 2.

	Volume (cm ³)		Number of Voxel		DSC (%)
	manual 1	manual 2	manual 1	manual 2	
Range	10.0	11.1	5866	6543	82.4
	122.6	117.7	70806	67963	92.6
μ	35.9	36.2			88.8
\pm	\pm	\pm	31294.8	31240.1	\pm
σ	30.0	28.7			3.3

Tab. 3. Direct comparison of manual slice-by-slice segmentations from physician 1 and physician 2 for twelve ablation zones via the DSC.

Moreover, we differentiated between the cases where the RF electrodes were still visible and the cases where the RF electrodes have already been removed, but found no significant differences between these. In more detail, the DSC values between readers were significantly higher ($p < 0.01$) than those between automatic and manual processing: 88.8% vs. 77.0%, also independent of whether the needle was still included (86.8% vs. 75.9%, $p < 0.05$) in the dataset or not (90.9% vs. 78.1%, $p < 0.05$), respectively. Segmented volumes appeared to be smaller with automatic processing than for readers, but mean differences were not significant: 33.03 ml vs. 36.02 ml ($p = 0.308$). This also held for cases with the needle included (25.76 ml vs. 25.93 ml, $p = 0.917$) and without (40.30 ml vs. 46.10 ml, $p = 0.249$). The mean DSC value of both readers appeared to be smaller when the needle was present (75.9% vs. 78.1% without, $p = 0.423$) but the difference was not significant. In contrast, the inter-observer DSC was significantly higher when the needle was not present (90.9% vs. 86.8%, $p = 0.025$). Statistical differences in DSC

values and segmentation volumes between methods were analyzed with Wilcoxon signed-rank tests, differences between both subgroups (with and without needle present) with a Mann-Whitney test. All analyses were done with SPSS (Version 20, IBM) using a level of significance of 0.05. However, the main difference between the automatic and manual segmentation is the computation time. Using the proposed automatic tool the segmentation was done in few seconds whereas the manual segmentation took on average 48 seconds – 8 min16 seconds (mean 3 min13 seconds).

IV. CONCLUSIONS

RFA of liver tumors induces areas of tissue necrosis, which can be visualized reliably in contrast enhanced CT. In this study, an interactive segmentation algorithm was applied to datasets of routine control CT scans after RFA of liver cancer for semi-automatic determination of thermally induced lesions. The segmentation accuracy was found to be sufficient for lesion segmentation in most of the cases although the manual segmentation still provided the best segmentation accuracy. The main advantage of the proposed tool over manual segmentation is its speed, which makes it an appealing alternative for physicians. As discussed, a minimally invasive RFA technique can stand an alternative to an open surgery and might also be suitable for patients who are inoperable. In RFA, post-interventional imaging is regularly performed to document the success of the treatment. When the interventional radiologist presumes that continuing of the therapy might be necessary, the RFA needle may still reside in the target organ during image acquisition. Due to hardening artefacts, image quality can be compromised significantly. However, these datasets have also been segmented and included into the study. For the evaluation of the contouring algorithm, manual slice-by-slice segmentations have been performed by two radiological experts, which enabled the DSC calculation between the manual and the semi-automatic segmentation outcome. Furthermore, we will provide the unique datasets – including the manual segmentations – to the community for their own research purposes. In summary, the achieved research highlights of the presented work are:

- Applying an interactive segmentation algorithm to RFA datasets from the clinical routine;
- Incorporating post-interventional patient acquisitions with and without RFA needles into the evaluation set;
- Performing pure manual slice-by-slice segmentations by clinical experts for quantitative and qualitative evaluation;
- Calculation of the Dice Similarity Coefficient for statistical validation of the presented segmentation algorithm;
- Providing the anonymized RFA data collection with the corresponding manual expert segmentation to the research community.

For comparison of our employed method with a state-of-the-art segmentation approach we applied the GrowCut implementation in 3D Slicer (www.slicer.org) to our data. The implementation is very user friendly because it does not require any precise parameter setting, rather the user initialize the method by marking areas in the image with simple strokes (Fig. 4.). Furthermore, we had good experiences with certain types of brain tumors (Glioblastoma multiforme (GBM) [18] and pituitary adenomas [19]). However, especially the cases where the needles are still in place – and thus visible within the images – caused massive problems (Fig. 5.). What happens is, that GrowCut leaks along the needles, because it cannot handle the large gray value differences between the ablation zone (dark) and the RFA needle (bright). Moreover, the initialization of GrowCut (marking parts of the lesion and the background) takes for a trained user between 30 and 60 seconds, in contrast to our method that needs only a single seed point. In addition, the user has to wait several seconds for the GrowCut segmentation result (on the same PC we used for interactive method about 10 seconds), where our method provides the segmentation result immediately in real-time. This makes a refinement much more convenient. Note: the sharp edges of the GrowCut result (green) in the rightmost image of Fig. 4. occur, because the Slicer implementation restricts the segmentation area with a bounding box. The size of the bounding box depends on the initialization of the user and avoid GrowCut to use the whole image or volume for the automatic segmentation process.

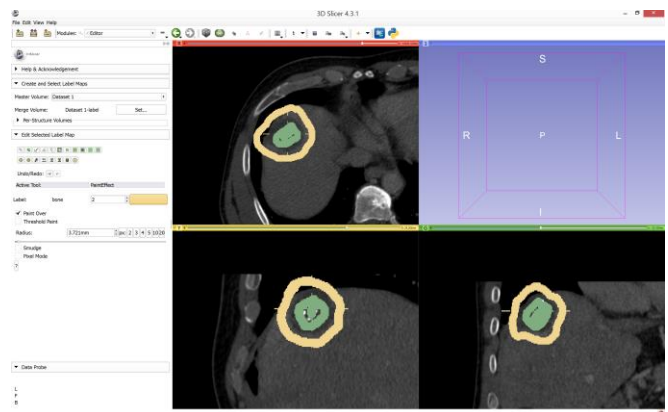


Fig. 4. GrowCut initialization for the segmentation of RF ablation zone: the ablated zone is marked in green and the background is marked in yellow on three 2D slices, respectively.

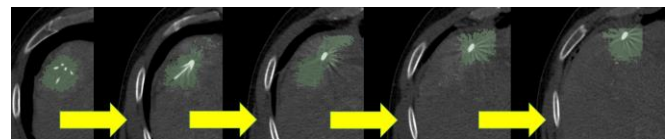


Fig. 5. GrowCut segmentation result (green) for the initializing from Fig. 4. The GrowCut segmentation leaks along the RFA needle, because it cannot handle the large gray value differences between the ablation zone (dark) and the needle (bright). Note: the sharp edges of the segmentation result in the rightmost image occur, because the GrowCut implementation under 3D Slicer automatic restricts the segmentation area with a bounding box that depends on the user initialization.

There are several areas for future work: we plan to integrate the interactive segmentation algorithm into a medical application framework for supporting ablation therapy. This is currently being developed within a project funded by the European FP7 program and is based the continuation on the European project IMPACT (Image-based Multi-scale Physiological Planning for Ablation Cancer Treatment, grant agreement no. 223877) [20] (<http://www.imppact.eu/>). In particular, our semi-automatic algorithm is targeted for the segmentation of difficult cases where an automatic segmentation fails. Moreover, we plan to provide the datasets acquired during the duration of the project over the next years. Furthermore, we want to investigate the possibilities for liver tumor tracking after one or several radiofrequency ablation interventions and support the needle placement [21] with our real-time segmentation algorithm and motion tracking [22].

ACKNOWLEDGMENT

This work received funding from the European Union in FP7: Clinical Intervention Modelling, Planning and Proof for Ablation Cancer Treatment (ClinicIMPACT, grant agreement no. 610886) and Generic Open-end Simulation Environment for Minimally Invasive Cancer Treatment (GoSmart, grant agreement no. 600641). Dr. Xiaojun Chen receives support from NSFC (National Natural Science Foundation of China) grant 81171429. Dr. Bernhard Kainz is supported by an EU FP7 MC-IEF 325661 grant.

REFERENCES

- [1] G. Graf et al., "Multimodal treatment of hepatocellular carcinoma," in *Eur J Intern Med*, Mar 22 2014.
- [2] S. L. Wong et al., "American Society of Clinical Oncology 2009 clinical evidence review on radiofrequency ablation of hepatic metastases from colorectal cancer," *J Clin Oncol*. 28, 493-508, 2010.
- [3] K. Passera, et al., "Radiofrequency ablation of liver tumors: quantitative assessment of tumor coverage through CT image processing," *BMC Medical Imaging*, 13, 2013.
- [4] E. S. McCreedy, et al., "Radio frequency ablation registration, segmentation, and fusion tool," *IEEE Trans Inf Technol Biomed*. 10, 490-6, 2006.
- [5] S. Keil, et al., "Semiautomated versus manual evaluation of liver metastases treated by radiofrequency ablation," *J Vasc Interv Radiol*. 21, 245-51, 2010.
- [6] A. Weihusen, et al., "Workflow oriented software support for image guided radiofrequency ablation of focal liver malignancies," *Proc. of the SPIE Medical Imaging*, 6509, article id 650919, 2007.
- [7] J. Kuhnigk, et al., "Fast automated segmentation and reproducible volumetry of pulmonary metastases in CT-scans for therapy monitoring," *Proc. of MICCAI*, 3217, 933-941, 2004.
- [8] I. Bricault, et al., "Liver metastases: 3D shape-based analysis of CT scans for detection of local recurrence after radiofrequency ablation," *Radiology* 241, 243-50, 2006.
- [9] D. Stippel, et al., "Variability of size and shape of necrosis induced by radiofrequency ablation in human livers: a volumetric evaluation," *Ann Surg Oncol*. 11, 420-5, 2004.
- [10] C. Schumann, et al., "State of the art in computer-assisted planning, intervention, and assessment of liver-tumor ablation," *Crit Rev Biomed Eng*. 38, 31-52, 2010.
- [11] B. Kainz, et al., "High-Resolution Contrast Enhanced Multi-Phase Hepatic Computed Tomography Data from a Porcine Radio-Frequency Ablation Study," *IEEE ISBI*, Beijing, China, 2014.
- [12] J. Egger, et al., "Nugget-Cut: A Segmentation Scheme for Spherically- and Elliptically-Shaped 3D Objects," *DAGM* 6376, 383-392, 2010.
- [13] Y. Boykov, and V. Kolmogorov, "An Experimental Comparison of Min-Cut/Max-Flow Algorithms for Energy Minimization in Vision," *IEEE PAMI* 26, 1124-1137, 2004.
- [14] J. Egger, et al., "Pituitary Adenoma Segmentation", *Proc. of Inter. Biosignal Processing Conf.*, Paper-ID 061, 1-4, 2010.
- [15] J. Egger, "PCG-Cut: Graph Driven Segmentation of the Prostate Central Gland," *PLoS One* 8, e76645, 2013.
- [16] J. Egger, et al., "Interactive-Cut: Real-Time Feedback Segmentation for Translational Research," *Comp Med Imaging Graph* 38, 285-95, 2014.
- [17] J. Egger, et al., "Manual Refinement System for Graph-Based Segmentation Results in the Medical Domain" *J Med Syst*. 36, 2829-39, 2012.
- [18] J. Egger, et al., "GBM Volumetry using the 3D Slicer Medical Image Computing Platform," *Sci Rep*. 3, 1364, 2013.
- [19] J. Egger, et al., "Pituitary Adenoma Volumetry with 3D Slicer," *PLoS ONE* 7, e51788, 2012.
- [20] B. Kerbl, et al., "Intervention Planning of Hepatocellular Carcinoma Radio-Frequency Ablations," *Clinical Image-Based Procedures. From Planning to Intervention*, Lecture Notes in Computer Science Volume 7761, 9-16, 2013.
- [21] X. Chen, et al. "Application of a surgical navigation system in rehabilitation of maxillary defects using zygoma implants: Report of one case," *The International Journal of Oral & Maxillofacial Implants*. 26(5):29-34, 2011.
- [22] X. Chen, et al., "Real-time motion tracking in image-guided oral implantology," *The International Journal of Medical Robotics and Computer Assisted Surgery*. 4(4):339-347, 2008.